DISLOCATION GENERATION AND CELL FORMATION AS A MECHANISM FOR STRESS CORROSION CRACKING MITIGATION

Paper #114

Grant Brandal[1], Y. Lawrence Yao[1]

[1] Advanced Manufacturing Lab, Columbia University
New York, NY 10027, United States

Abstract

The combination of a susceptible material, tensile stress, and corrosive environment results in stress corrosion cracking (SCC). Under these suitable conditions, brittle and catastrophic failure occurs at levels much lower than the material's ultimate tensile strength. While several different mechanisms of failure occur for SCC, hydrogen from the corrosive environment penetrating into the lattice is often a common theme. Laser shock peening (LSP) has previously been shown to prevent the occurrence of SCC on stainless steel. Compressive residual stresses from LSP are often attributed with the improvement, but this simple explanation does not explain the electrochemical nature of SCC by capturing the effects of microstructural changes from LSP processing and its interaction with the hydrogen atoms on the microscale.

As the hydrogen concentration of the material increases, a phase transformation from austenite to martensite occurs. This transformation is a precursor to SCC failure, and its prevention would thus help explain the mitigation capabilities of LSP. In this paper, the role of LSP induced dislocations counteracting the driving force of the martensitic transformation is explored. Stainless steel samples are LSP processed with a range of incident laser intensities and overlapping. Cathodic charging is then applied to accelerate the rate of hydrogen absorption. Using XRD, martensitic peaks are found after 24 hours in samples that have not been LSP treated. But martensite formation does not occur after 24 hours in LSP treated samples. Transmission electron microscopy is used for determining the resulting structure and dislocation densities. The arrangement of the dislocations, for example forming cell like structures, is important to the hydrogen trapping capabilities. A finite element model predicting the dislocation density and cell formation is also developed to aid in the interpretation.

Introduction

Material failure by corrosion can often be prevented because corrosive products, such as rust, indicate that the integrity of the material has weakened. But a special case of corrosion called Stress Corrosion Cracking (SCC) behaves quite differently from conventional corrosion. SCC occurs when a susceptible material in a suitable corrosive environment experiences a tensile stress. The required stress can be either externally applied or residual stress from a previous manufacturing process, and levels as low as 20% of the material's yield strength have been shown to cause failure [1]. Of most concern with SCC is that it causes sudden and catastrophic material failure. Additionally, materials generally thought of as being resistant to corrosion are susceptible to SCC failure in certain environments and furthermore it is quite difficult to predict when the onset of SCC is going to occur.

Many different industrial applications are prone to experiencing SCC. Considerable attention has been paid to the occurrence of SCC in the boiling water reactors found in nuclear power plants [2], where any failures could result in extremely dangerous situations. Pressure vessels and gas pipelines have been found to be at risk [3,4], as are various types of implantable medical devices [5].

Various physical descriptions exist for explaining the mechanisms of SCC, but they often are related to deleterious effects of hydrogen atoms absorbed from the corrosive environment. In this case, the term hydrogen embrittlement is used. Hydrogen has a high diffusivity in metals, and it is highly reactive with the material's lattice. Processes such as electroplating, pickling, or various types of surface cleaning can further increase the levels of absorbed hydrogen within the lattice. Details on the physical changes to the material's lattice and structure will be provided in the following section.

To prevent material failure by SCC, several different mitigation techniques exist. Coating and plasma

nitriding of the material can prevent surface reactions and limit the amount of hydrogen that penetrates into the lattice [6,7], but in harsh environments coatings will eventually degrade and since they are not as tough as the metal, may crack or delaminate leaving the material vulnerable to SCC. A different approach to mitigation is to actually modify the material itself, by imparting a compressive residual stress on the material's surface. One such technique is laser shock peening (LSP), which uses incident laser pulses to generate shockwaves on a material's surface. While originally developed for increasing the fatigue life of metallic components [8], recent studies have shown that LSP processing helps to prevent the onset of SCC [9,10]. The improvement has mostly been attributed to the compressive stress counteracting the necessary tensile stress for SCC initiation, but this cannot be solely attributable, as evidenced by the fact that LSP processing can decrease the corrosion current of 4140 steel [11], an electrochemical effect. LSP causes many forms of microstructural changes to the material, including the generation of lattice dislocations and sub grain dislocation cell formation [12]. Lattice dislocations act as hydrogen trapping sites and will influence the absorption and diffusion of hydrogen [13], and structural changes to the lattice symmetry will further influence SCC occurrence. In this paper we identify the underlying microstructural changes to stainless steel 304 induced by LSP that allow for it to be a beneficial mitigation process against SCC.

Background

Microstructural Considerations for SCC

Of particular concern for SCC in stainless steels is the formation of martensite, a phase that is brittle and susceptible to fracture and corrosion [14]. The fracture surfaces of initially austenitic stainless steel that has failed by SCC show that brittle failure has occurred, which is most often accompanied by the presence of martensite on the fracture surface [15,16]. Even materials that initially are fully austenitic can from martensite through various environmental processes, thereby weakening the material [17]. Martensite is characterized as a phase that forms via a diffusionless transformation, which in the case of stainless steel, the initially FCC austenite transforms into martensite which can be of either BCC or HCP crystal systems. In carbon steel systems, this transformation occurs upon rapid cooling from elevated temperatures [18]. This does not allow time for carbon to diffuse, and the remaining carbon atoms sit in interstitial lattice sites, causing distortions and subsequently the phase change. In corrosive environments, the same type of lattice transformation from austenite to martensite occurs, except that it is now hydrogen atoms causing the lattice distortions and internal stress. During exposure to the corrosive environment, once this transformation has occurred, even locally, the likelihood of brittle failure is greatly enhanced. Therefore, prevention of the martensitic transformation would be a powerful method for mitigation of SCC failure in austenitic stainless steels.

Olson and Cohen described the initiation sites for martensite as the intersection of shear bands and identified which lattice planes the transformation will occur on [19]. As hydrogen from the corrosive environment diffuses into austenite, it causes expansion and an internal stress that acts as a driving force for the formation of martensite. This strain energy increases the free energy of the austenite, subsequently making the martensite phase more stable. Plots of the free energy of the respective phases are shown vs. temperature in Figure 1, where ΔG_{ch} is the difference in chemical free energy of the two phases.

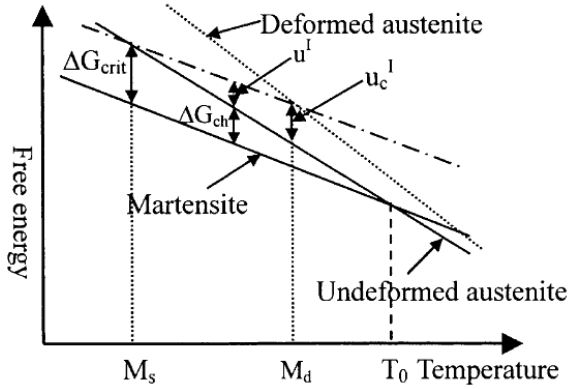

Figure 1 Free energy diagram showing the suitable conditions for the formation of deformation induced martensite [20].

In stainless steels, the addition of alloying elements promotes the formation of austenite, so that in Figure 1 T_0 can be below room temperature. For the stress induced martensitic transformation to occur, the internal stain energy must be equal to ΔG_{crit}-ΔG_{ch}. Martensite becomes the lower energy phase with increasing amounts of absorbed hydrogen because the BCC and HCP lattices provide more interstitial spaces for the hydrogen to reside [21,22], but this is also accompanied by a volumetric expansion of nearly 4%.

Since the martensitic transformation requires significant levels of hydrogen to reach the required strain energy, accelerated testing by cathodically charging the workpiece is often performed. X-Ray Diffraction, which measures lattice spacing, is a preferred method for detecting phases present in a

metallic sample. Narita et al. have used this method to identify the formation of martensite, as well as relating lattice shifts of the austenite peaks to expansion caused by absorbed hydrogen [23].

Laser Shock Peening and Lattice Changes

Generating shockwaves on the surface of a metallic sample causes plastic deformation and a residual compressive stress. While this can be performed with processes such as mechanical shot peening, a more effective method which provides effects deeper into the surface is laser shock peening (LSP). In LSP, the workpiece is coated with an ablative layer and then a confining medium transparent to the laser is placed on top. Upon laser irradiation, the ablative layer is ionized and a plasma cloud forms. This wants to expand, but the confining medium restricts the expansion and thus a shockwave is generated that propagates down into the material, resulting in a residual compressive stress within the material. Since the laser is completely absorbed in the ablative layer, no thermal effects are caused in the workpiece, which is especially important for SCC considerations because any heat affected zone (HAZ) in the material could negatively affect its corrosion resistance. Rastering the laser beam across the workpiece allows larger areas to be processed.

Upon LSP processing, many lattice changes are induced within the workpiece, altering the behavior and effect of absorbed hydrogen within the lattice, and can be responsible for the SCC mitigation performance of LSP. Plastic deformation is accompanied with the generation of lattice dislocations, where LSP has been shown to cause large increases in dislocation density. Hydrogen diffusing through a crystal lattice gets stuck in the dislocations, known as hydrogen trapping. This effectively reduces the diffusivity of hydrogen within the material while also increasing its solubility by providing low energy places for the hydrogen to reside.

A unique feature of dislocations is the way that they will interact and tangle with each other. With increasing amounts of deformation, this tangling will result in the formation of dislocation cells [24] The periodic dislocation cell structure has walls of high dislocation density and interiors of lower densities, and these cells are present within individual grains of the polycrystals. Dislocation cell formation has been experimentally detected using micro-XRD measurements that provide micron level spatial resolution [12], as well as TEM imaging showing the cellular structure [25]. LSP processing introduces additional considerations for the theory of dislocation generation, because it causes incredibly high strain rates. Since dislocation multiplication is often considered as the result of tangling dislocations (such as Frank-Read sources), it cannot account for the whole phenemonon of LSP dislocation generation because it would require dislocations within the lattice to be traveling at speeds higher than physically possible in order to keep up with the wave front. To rectify this, Meyers and Murr proposed [26] a mechanism of homogenous dislocation generation, as expressed in Equation 1, which does not require dislocation motion to keep up with the wave front for generation.

$$\tau_h = 0.054G \tag{1}$$

Where τ_h is the shear stress required for homogeneous generation, and G is the shear modulus. At the wave front high shear stresses do form, and by this equation it is indicated this additional mechanism for dislocation generation will result in high dislocation densities from LSP, increasing the hydrogen trapping capability of shock wave processed materials.

Numerical Modelling

Using finite element methods, a numerical model was implemented for obtaining the dislocation density and cell size induced by various levels of LSP processing. The high strain rates in LSP require that the material be analyzed with hydrodynamic considerations [27]. Rather than the usual Hooke's law governing deformation, the Mie-Gruneisen equation of state has been implemented, relating energy to internal pressure as:

$$p - p_H = \Gamma_o \rho_o (E_m - E_H) \tag{2}$$

where p is pressure, p_H is the Hugoniot pressure, E_H is the Hugoniot energy, ρ_o is the reference density, and Γ_o is a material constant. Combining this with the Hugoniot jump conditions results in [28]:

$$p = \frac{\rho_o c_o^2 \eta}{(1-s\eta)^2}\left(1 - \frac{\Gamma_o \eta}{2}\right) + \Gamma_o \rho_o E_m \tag{3}$$

for c_o and s the Hugoniot parameters and $\eta = 1 - \rho_o/\rho$. The incident laser pulse was simulated as a spatio-temporal pressure on the top surface, with the value calculated by [8]:

$$P = A\left(\frac{\alpha}{2\alpha+3}\right)^{1/2}\sqrt{Z * I} \tag{4}$$

Where P is the exerted pressure from the shock wave, A is a constant, $\alpha \approx 0.1$, Z is the shock impedance, and I is the laser intensity. As discussed in the preceding section, during deformation the generation of

dislocations and their subsequent arrangement into cellular structures will influence the behavior of hydrogen within the lattice. Toth et al. derived equations for the rate of dislocation generation with deformation as [29]:

$$\frac{d\rho_w}{dt} = \frac{6\beta^*\dot{\gamma}_c(1-f)^{2/3}}{bdf} + \frac{\sqrt{3}\beta^*\dot{\gamma}_c(1-f)\sqrt{\rho_w}}{fb} - k_o\dot{\gamma}_w\rho_w\left(\frac{\dot{\gamma}_w}{\dot{\gamma}_o}\right)^{-1/n} \quad (5)$$

$$\frac{d\rho_c}{dt} = \alpha^*\frac{\dot{\gamma}_w\sqrt{\rho_w}}{b\sqrt{3}} - \beta^*\frac{6\dot{\gamma}_c}{bd(1-f)^{1/3}} - k_o\dot{\gamma}_c\rho_c\left(\frac{\dot{\gamma}_c}{\dot{\gamma}_o}\right)^{-1/n} \quad (6)$$

where ρ is the dislocation density with subscript w for cell walls and c for cell interior, α* and β* are constants, f is the volume fraction of the cell walls vs. cell interior, b is burgers vector, d is the lattice spacing, and $\dot{\gamma}$ is the shear strain rate. These equations are incrementally solved during shock wave propagation and relaxation to determine the distribution and density of dislocations.

Experimental Setup

AISI 304 stainless steel samples were used as the workpieces. A Continuum NY61 pulsed Nd:YAG laser with a wavelength of 1064 nm, pulse energies ranging from 125 – 300 μJ, spot size of 1 mm, and pulse lengths of 17 ns was used for the LSP processing. In the experimental configuration, the ablative layer was black electrical tape and the confining medium of clear acrylic was clamped on top. For the TEM imaging, a FEI Talos F200X S/TEM was used. Specimen preparation for the TEM was performed on a FEI Helios NanoLab 660 SEM/FIB using the lift-out technique. Cathodic charging of the samples in 1M sulfuric acid at a current density of 50 mA/cm2 for up to 48 hours was also performed, and lattice spacing and phase detection was carried out in a PANAlytical XPert3 Powder XRD. The finite element analysis was implemented in ABAQUS.

Results & Discussion

Detection of Martensite Formation

Characterization of the microstructural changes induced by absorbed hydrogen within the lattice have been performed by making XRD measurements on stainless steel samples that underwent cathodic charging. Figure 2a shows a selected portion of the XRD spectrum of the AISI 304 prior to any cathodic charging, and is thus our reference state. The two peaks present at 43.45° and 50.68° are both austenitic and correspond to the (111) and (200) orientations,

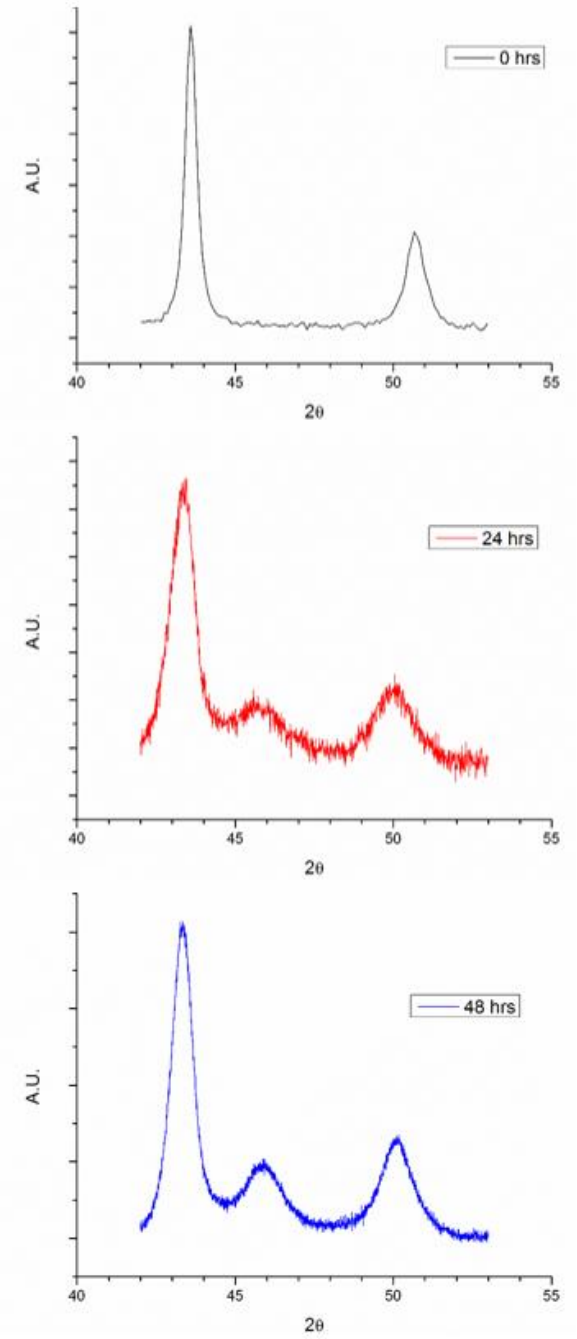

Figure 2 XRD measurements of lattice changes from cathodic charging a specimen without LSP treatment. Prior to cathodic charging, the material is fully austenitic (a). After 24 hours (b), the absorbed hydrogen has caused the formation of a martensite peak, with further increases after 48 hours (c)

respectively. Full spectrum scans for 2θ values up to 110° were performed to ensure that the material is fully austenitic, but only the selected spectrum of 42° to 53° is presented in the figures because this is the region where most of the induced changes are found to occur.

After 24 hours of cathodic charging distinct microstructural changes occurred in the sample, as seen in Figure 2b. A new peak at 45.98° is present, which corresponds to ε-martensite. As no thermal or mechanical processes have been used, this phase transformation is strictly a result of the cathodic charging and subsequent hydrogen absorption. Once this transformation has occurred, the stainless steel's susceptibility to premature failure by SCC is greatly enhanced. Figure 2c shows the same sample after 48 hours of total cathodic charging time, and the ε-martensite peak has become even more prominent. This increasing amount of martensite within the lattice simply further increases the material's SCC susceptibility.

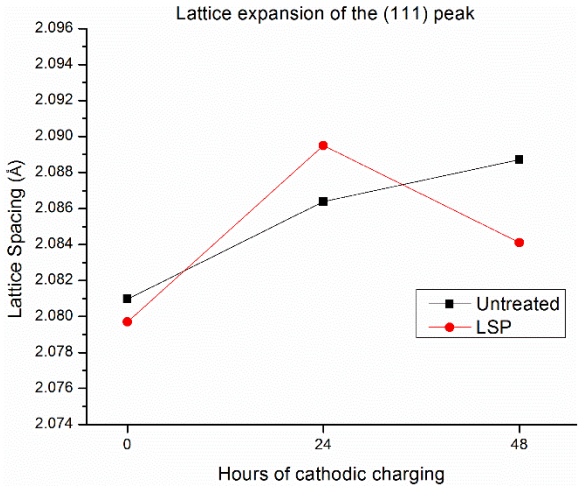

Figure 3 Hydrogen induced lattice expansion for 24 and 48 hours of cathodic charging.

As the austenite phases absorb hydrogen they undergo volume expansion, and this expansion is detected as peak shifts in the XRD spectrum, as seen in Figure 3. The change in lattice parameter can be expressed as [30]:

$$a_H = a_o + K \cdot C(x,t) \qquad (7)$$

where a_H is the lattice parameter after hydrogen absorption, a_o is the initial lattice parameter, K is a constant, and C(x,t) is the concentration of hydrogen. With consideration of Bragg's Law, increases in lattice parameters correspond to decreases in 2θ values. After 24 hours of cathodic charging, the (111) peak has shifted to 43.41°, and it has shifted to 43.28°after 48 hours. The steady expansion for the untreated sample in Figure 3 indicates the continued absorption of hydrogen.

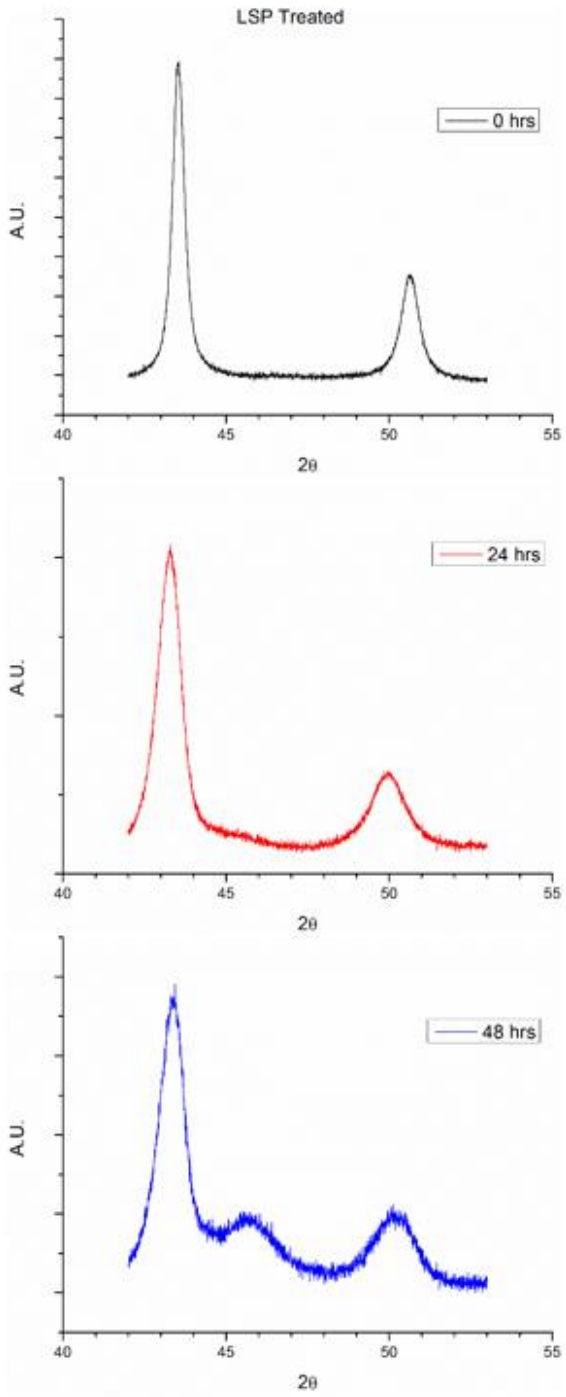

Figure 4 XRD measurements of a selected region of the spectrum for samples after LSP processing (a), and then subjected to 24 hours (b) and 48 hours (c) of cathodic charging. The initially austenitic peaks experience broadening after 24 hours, but no martensite formation occurs, illustrating the effectiveness of LSP processing as a mitigation tool. Some martensite does eventually form after 48 hours.

For analysis of the mechanism whereby SCC and hydrogen embrittlement can be mitigated, LSP treated samples were exposed to the same amount of cathodic charging, as presented in Figure 4. While it is possible for plastic deformation from the LSP processing to induce martensite, Figure 4a confirms that this transformation has not occurred during our processing. This image is after LSP treating the surface with 3 repetitions, and was subsequently placed into the cathodic charging configuration. After 24 hours of cathodic charging, shown in Figure 4b, the austenite peaks have slightly broadened (a result of distortions to the lattice), but no martensite peak has formed. This is in direct contrast to Figure 2b, and demonstrates that LSP processing suppresses martensite formation and thereby limits the stainless steel from SCC susceptibility. But, from Figure 3, the (111) peak has undergone greater expansion compared to the untreated sample after 24 hours. This is because no martensite is available in the LSP treated sample to accommodate hydrogen. The microstructural changes from LSP that provide this mitigation will be discussed in the following section. After continued cathodic charging for 48 hours of the LSP treated sample, ε-martensite eventually does begin to form, as shown in Figure 4c. But this figure is similar to the shape of Figure 2b. So even once martensite does begin to form in the LSP treated sample, the amount is still less than that of an untreated sample, and therefore also less likely to suffer premature failure. In Figure 3 the lattice expansion of (111) has now significantly decreased from the value at 24 hours, indicative of how the deformed austenite no longer needs to retain as large of amounts of hydrogen and can thus relax.

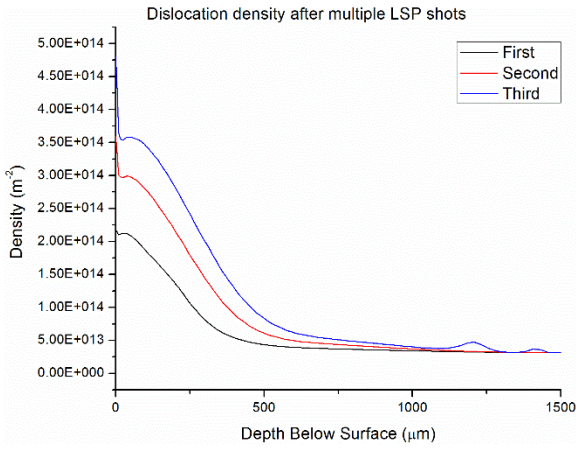

Figure 5 Increases to the dislocation density after LSP processing, which act as an impediment to hydrogen induced martensite formation. The largest increase is seen upon the initial incident pulse.

Mechanism of SCC Mitigation

LSP processing causes numerous changes to the microstructure of the material, but perhaps most importantly to the mitigation of SCC is increases of dislocation density. Figure 5 shows the dislocation density as a function of depth below the surface after one, two, and three LSP impacts as determined by the finite element model. Increases of nearly 4 times are induced by the first pulse, with decreasing amounts of gains for the following pulses. The increase decays with depth into the sample, with the extent of the effects reaching nearly 1 mm, for which the scale is similar to the other reports of the depths of plastic zones in LSP. Mitigation benefits are provided by dislocations because when they tangle they will restrict motion within the lattice, particularly the coordinated lattice movement required for the martensitic transformation to occur. Chatterjee et al. developed a theory describing this stabilization of the austenite phase, expressed as [31]:

$$\Delta G = \frac{1}{8\pi(1-\nu)}\mu b\sqrt{\rho} + \tau_s \qquad (8)$$

where ΔG is the magnitude of the driving force required for transformation, ρ is the dislocation density, μ is the shear modulus, b is burgers vector, and τ_s is shear stress from solution hardening. By increasing the density of dislocations, a larger driving force is required, which in the case of SCC means that larger amounts of hydrogen within the lattice are required for the detrimental phase transformation to occur.

A second effect caused by the increase of dislocation density is a result of dislocations behaving as hydrogen trapping sites, altering both the diffusivity and solubility of hydrogen within the material's lattice. Decreasing the diffusivity will result in the hydrogen not being able to penetrate deep into the material and

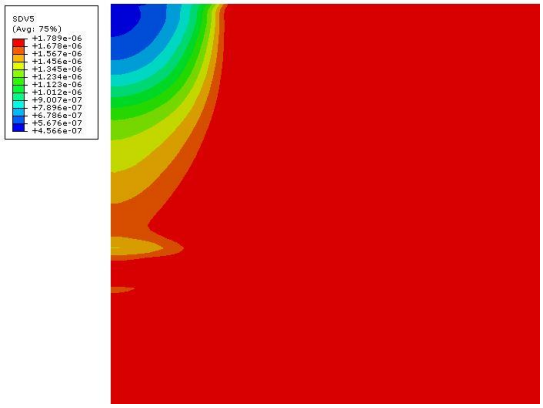

Figure 6 Distribution of dislocation cell size after 3 LSP impacts. Symmetry is used along the boundary at the left side.

restrict any hydrogen induced changes to the near surface level. Additionally, hydrogen residing in trapping sites will cause less internal stress within the lattice and therefore be less likely to cause brittle failure. The formation of dislocation cells by LSP processing can provide further restrictions to martensitic formation. Figure 6 shows a 2D cross section of the dislocation cell size after 3 incident LSP pulses, with symmetry being used along the left hand boundary. An initial distribution of a cellular arrangement is required for the model, but this is set to 1.8 μm which is large enough that it can nearly be considered to be the grain size. Again since the hydrogen induced martensitic transformation requires coordinated lattice movement, microstructural disruptions can prevent the transformation. The martensitic transformation will not propagate across grain boundaries, and in the same way dislocation cells may prevent propagation as well. Along grain boundaries misorientation creates high diffusivity paths for hydrogen to penetrate, but dislocation cells are not associated with misorientation, and therefore dislocation cells may be further advantageous over grain boundaries.

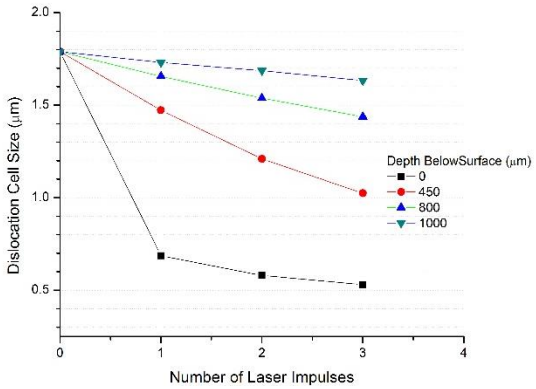

Figure 7 Dislocation cell size for increasing number of incident LSP pulses at 4 depths.

Figure 7 presents the dislocation cell size at various depths below the surface for increasing numbers of LSP impacts. Similar to the dislocation density, the greatest change in cell size are caused by the first laser pulse, especially near the surface. But at 450 μm deep, the cell size continues to decrease after the second and third pulses. This suggests that further increases to the number of incident pulses will help to cause deeper effects of cell formation, but a minimum cell size will be eventually attained.

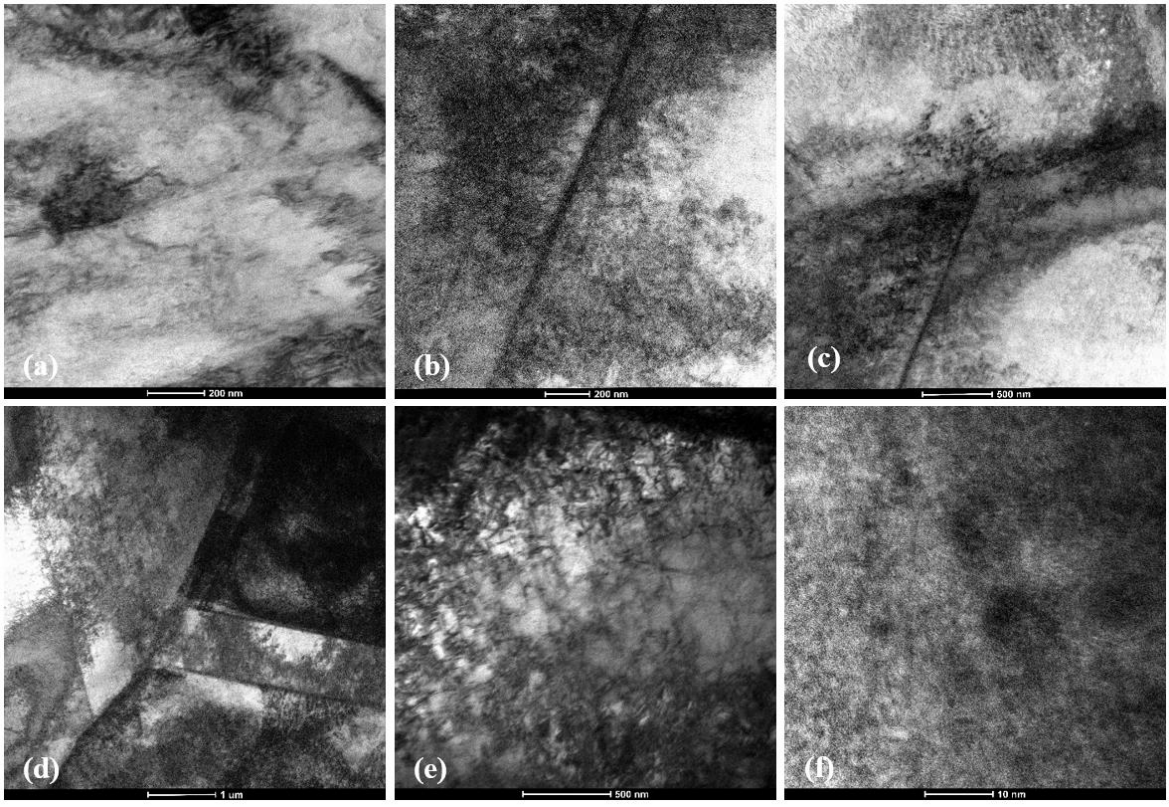

Figure 8 TEM images of untreated AISI 304 stainless steel (a), after 3 LSP impacts at 2.25 GW/cm^2 (b-f). Significant increased to the dislocation density are seen in (b), and these dislocations get tangled at grain boundaries (c). The individual grains in (d) have differing dislocation behaviour. Cell formation is present in (e), and the high magnification of (f) shows the orientation of the lattice.

Imaging Analysis

TEM images of the stainless steel samples at various magnifications are provided in Figure 8. Even before LSP treating, low concentrations of dislocations are present in the samples, as seen in Figure 8a. This loosely aligned structure corresponds to the assumption of an initial concentration that was used for defining the FEM model. Annealing of the samples would provide further reductions in the initial dislocation density if desired.

After LSP processing, a significant increase in the dislocation concentration is detected as shown in Figure 8b at the same magnification as Figure 8a. This sample has been processed with 3 LSP pulses, where the dark line running through the center of the image is a grain boundary. The darker regions of the image correspond to dense dislocation tangling, and some regions with low dislocation densities are found on the right hand side. Stress concentrations are the contributor to this uneven distribution. Dislocation behavior between neighboring grains may be significantly different because the dislocations will not diffuse across the grain boundary and since the grains have different rotational orientation to the direction of loading, the slip systems that have become activated will not be the same. Dislocations in Figure 8c can clearly be seen accumulating near the grain boundary, with discontinuities in density across the boundary.

Decreasing the magnification, as done in Figure 8d, shows even more dramatically the non-homogeneity between adjacent grains. Furthermore, the grain in the upper portion of this image shows a periodic structure for the tangling of dislocations and thus indicates that some dislocation cell formation has occurred. A magnified image of one such region is shown in Figure 8e. These dislocation cells effectively partition the inner regions of the grain, helping to prevent the propagation of any martensitic transformation. Performing high resolution TEM enables the direct observation of the material's lattice, albeit with sacrificing the size of area covered. In Figure 8f, obtained at 1M X, lattice orientations at various angles are seen.

The results from these TEM images are consistent with the previous analysis from both the phase detection and finite element analyses. Significant increases in dislocation density, as determined in Figure 5, are found and this increase helps to restrict the driving force for the martensitic transformation. Dislocation cell walls may prevent the coordinated movement required for the martensitic transformation, so that if a region does begin to transform it will be restricted to small, localized areas. At high levels of deformation, it is possible for LSP to induce grain refinement, where the increased grain boundaries with high amounts of misorientation will provide high diffusivity paths for the hydrogen to deeply penetrate the lattice. Figure 9 shows a TEM diffraction pattern obtained in a region with dislocation cell structures similar to Figure 8e. For polycrystalline regions, the diffraction pattern would show concentric rings indicative of the various orientations of each lattice structure [25]. But the singular alignment of the diffraction pattern indicates that there is not any misalignment across the boundaries, thereby ensuring that high hydrogen diffusivity paths are not formed.

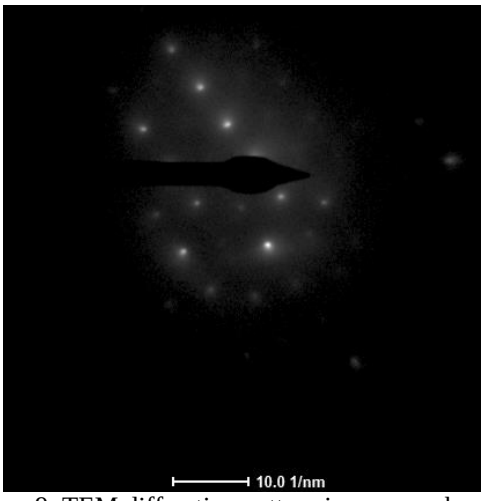

Figure 9 TEM diffraction pattern in an area showing dislocation cell structure, indicating that there is not lattice misalignment across the boundaries.

Conclusion

As hydrogen from a corrosive environment penetrates into the lattice of stainless steel, it can induce a phase change of the material from austenite to martensite. This phase change then dramatically increases the material's susceptibility to failure by SCC. We have shown that laser shock peening is an effective process for preventing this transformation, and thus improving stainless steel's resistance to SCC. The increases to dislocation density induced by LSP processing restrict the driving force of the transformation

Acknowledgement

We would like to acknowledge Columbia University's Nanoscience Initiative for the use of its shared facilities, and the Fu Foundation School of Engineering and Applied Science and the Faculty of Arts & Sciences for their support of the CNI Facilities.

Additional support from Columbia University is also gratefully acknowledged.

References

[1] Lijie, Q., Wuyang, C., Huijun, M., Jimei, X., and Peixin, G., 1993, "Hydrogen-facilitated corrosion and stress corrosion cracking of austenitic stainless steel of type 310," MetTrans A, **24**, pp. 959–962.

[2] Was, G. S., and Andresen, P., 2007, "Stress Corrosion Cracking Behavior of Alloys in Aggressive Nuclear Reactor Core Environments," Corrosion, **63**(1), pp. 19–45.

[3] Manfredi, C., and Otegui, J. ., 2002, "Failures by SCC in buried pipelines," Eng. Fail. Anal., **9**(5), pp. 495–509.

[4] Kane, R. D., Sridhar, N., Brongers, M. P., Beavers, J. A., Agrawal, A. K., and Klein, L. J., 2005, "Stress corrosion cracking in fuel ethanol: a recently recognized phenomenon," Mater. Perform., (12), pp. 50–55.

[5] Manivasagam, G., Dhinasekaran, D., and Rajamanickam, A., 2010, "Biomedical Implants: Corrosion and its Prevention - A Review," Recent Patents Corros. Sci., **2**(1), pp. 40–54.

[6] Ensinger, W., 1996, "Ion-beam sputter coating of tantalum tube inner walls for protection against hydrogen embrittlement," Surf. Coatings Technol., **84**(1-3), pp. 434–438.

[7] Michler, T., 2008, "Influence of plasma nitriding on hydrogen environment embrittlement of 1.4301 austenitic stainless steel," Surf. Coatings Technol., **202**, pp. 1688–1695.

[8] Peyre, P., and Fabbro, R., 1995, "Laser shock processing : a review of the physics and applications," Opt. Quantum Electron., **27**, pp. 1213–1229.

[9] Zhang, Y., Lu, J., and Luo, K., 2013, "Stress Corrosion Cracking Resistance of AISI 304 SS Subjected to Laser Shock Processing," Laser Shock Processing of FCC Metals, Springer, Berlin, Germany, pp. 137–152.

[10] Brandal, G., and Yao, Y. L., 2015, "Microstructural Effects Induced by Laser Shock Peening for Mitigation of Stress Corrosion Cracking," ICALEO, Atlanta, GA.

[11] Peyre, P., Braham, C., Ledion, J., Berthe, L., and Fabbro, R., 2000, "Corrosion Reactivity of Laser-Peened Steel Surfaces," **9**(December), pp. 656–662.

[12] Chen, H., Yao, Y. L., and Kysar, J. W., 2004, "Spatially Resolved Characterization of Residual Stress Induced by Micro Scale Laser Shock Peening," J. Manuf. Sci. Eng., **126**(2), p. 226.

[13] Hirth, J. P., 1980, "Effects of Hydrogen on the properties of Iron and steel," Metall. Trans. A, **11**, pp. 861–890.

[14] Ozgowicz, W., Kurc-lisiecka, A., and Grajcar, A., 2012, "Corrosion Behaviour of Cold-Deformed Austenitic Alloys."

[15] Zinbi, A., and Bouchou, A., 2010, "Delayed cracking in 301 austenitic steel after bending process : Martensitic transformation and hydrogen embrittlement analysis," **17**, pp. 1028–1037.

[16] Liu, R., Narita, N., Alstetter, C., Birnbaum, H., and Pugh, E. N., 1980, "Studies of the Orientations of Fracture Surfaces Produced in Austenitic Stainless Steels By Stress-Corrosion Cracking and Hydrogen Embrittlement," Metall. Trans. A, **11**(September), pp. 1563–1574.

[17] Solomon, N., and Solomon, I., 2010, "Deformation induced martensite in AISI 316 stainless steel (•)," **46**(13), pp. 121–128.

[18] Kalpakjian, S., and Schmid, S., 2010, Manufacturing: Engineering and Technology, Pearson Prentice Hall, Upper Saddle River, NJ.

[19] Olson, G. B., 1972, "A mechanism for the strain-induced martensitic transformations* nucleation of," J. LessCommon Met., **28**(1), pp. 107–118.

[20] Shin, H. C., Ha, T. K., and Chang, Y. W., 2001, "Kinetics of deformation induced martensitic transformation in a 304 stainless steel," **45**, pp. 823–829.

[21] Vakhney, A. G., Yaresko, A. N., Antonov, V. N., and Nemoshkalenko, V. V, 1998, "The effect of hydrogen on the electronic structure and phase stability of iron-based alloys doped with chromium and nickel," **10**, pp. 6987–6994.

[22] Greeley, J., and Mavrikakis, M., 2003, "A first-principles study of surface and subsurface H on and in Ni (1 1 1): diffusional properties and coverage-dependent behavior," **540**, pp. 215–229.

[23] Narita, N., Altstetter, C. J., and Birnbaum, H. K., 1982, "Hydrogen-related phase transformations in austenitic stainless steels," Metall. Trans. A, **13**(8), pp. 1355–1365.

[24] Holt, D. L., 1970, "Dislocation cell formation in metals," J. Appl. Phys., **41**(8), pp. 3197–3201.

[25] Mordyuk, B. N., Milman, Y. V., Iefimov, M. O., Prokopenko, G. I., Silberschmidt, V. V., Danylenko, M. I., and Kotko, a. V., 2008, "Characterization of ultrasonically peened and laser-shock peened surface layers of AISI 321 stainless steel," Surf. Coatings Technol., **202**(19), pp. 4875–4883.

[26] Meyers, M., and Murr, L., 1981, Shock Waves and High Strain Rate Phenomena in Metals, Plenum Press, New York.

[27] Fan, Y., Wang, Y., Vukelic, S., and Yao, Y. L., 2007, "Numerical Investigation of Opposing Dual Sided Microscale Laser Shock Peening," J. Manuf. Sci. Eng., **129**(2), p. 256.

[28] Simulia, 6AD, "Abaqus Analysis User's Guide."

[29] Tóth, L. S., Molinari, A., and Estrin, Y., 2002, "Strain Hardening at Large Strains as Predicted by Dislocation Based Polycrystal Plasticity Model," J. Eng. Mater. Technol., **124**(1), p. 71.

[30] Rozenak, P., and Bergman, R., 2006, "X-ray phase analysis of martensitic transformations in austenitic stainless steels electrochemically charged with hydrogen," **437**, pp. 366–378.

[31] Chatterjee, S., Wang, H., Yang, J. R., and Bhadeshia, H. K. D. H., 2006, "Mechanical stabilisation of austenite," **22**(6), pp. 641–644.